ACS APPLIED NANO MATERIALS

www.acsanm.org Article

ZnO/Cellulose Nanofiber Composites for Sustainable Sunlight-Driven Dye Degradation

Mostafa Dehghani, Humayun Nadeem, Vikram Singh Raghuwanshi, Hamidreza Mahdavi, Mark M. Banaszak Holl, and Warren Batchelor*

Cite This: *ACS Appl. Nano Mater.* 2020, 3, 10284–10295 Read Online

ACCESS | Metrics & More | Article Recommendations | Supporting Information

ABSTRACT: Porous ZnO/cellulose nanofiber (CNF) composites were synthesized to investigate their photocatalytic degradation of methylene blue (MB) dye (a persistent organic pollutant model) under a UV lamp and sunlight. UV/vis analysis indicated that complete photodegradation was achieved in about 10 min under natural sunlight with low UV intensity (between 1500 and 2900 $\mu W/cm^{-1}$ of UVA/B). Scanning electron microscopy, Fourier transform infrared, Brunauer–Emmett–Teller, X-ray diffraction, and small-angle X-ray scattering characterization of the composite were consistent with flower/plate morphology ZnO nanomaterials of similar size to the CNF fiber diameter distributed in the matrix. The catalyst with 0.3 M $Zn(Ac)_2$ and 1.5 wt % CNF loading was the sample with the highest MB photodegradation efficiency of >99% in less than 10 min. This study provides proof-of-concept of a simple, sustainable, ecofriendly, and industrially scalable approach to synthesize extremely efficient ZnO/CNF photocatalysts for the degradation of organic pollutants. Catalyst performance showed greater dye degradation with a function of irradiation time as compared to state-of-the-art catalysts reported in the literature.

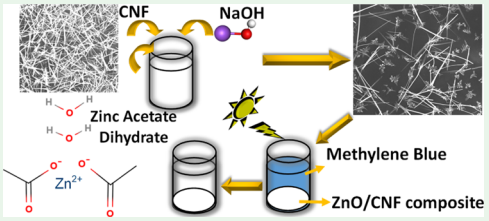

KEYWORDS: *dye degradation, photocatalyst, sunlight irradiation, ZnO/CNF composite, wastewater treatment, sustainable processing*

INTRODUCTION

The increase in global population has led to enhanced industrial activities and the uncontrolled release of persistent organic pollutants (POPs) into wastewater streams. This discharge into the environment is unacceptable as it results in the contamination of water supplies with compounds that are resistant to degradation through natural chemical, biological, and photolytic processes.[1] In recent years, novel technologies have been developed for the separation of a wide variety of pollutants such as dyes, pesticides, and heavy metals. Mechanisms include membrane distillation, photocatalytic degradation, adsorption, membrane separation, ion exchange, electrochemical methods (such as electrocoagulation and electrochemical reactors for metal recovery), electrodialysis, mechanical, and bioseparation processes.[2−6] Most of these methods are not effective for the degradation of organic effluents and in some cases they merely separate the pollutants, resulting in the formation of secondary wastes that still require treatment.[7] There is a pressing need to develop new techniques to reduce POPs in an environmentally friendly approach that does not require expensive energy input. Because of the low cost, ease of set-up, low maintenance, flexible production, and remarkable performance for removal of organic species, photocatalytic processes are strong sustainable candidates for the treatment of these types of wastewaters.[8,9] Table 1 summarizes various wastewater treatment processes and highlights that the photocatalytic process can be operated with lower cost and higher efficiency as compared to other treatment technologies. Based on the criteria presented in the literature (Table 1),[10−13] photocatalytic degradation of organic pollutants is one of the most sustainable processes.

Photocatalysis can be conducted using either artificial light (UV to near-visible wavelengths) or sunlight.[21] The use of UV lamps have gained considerable attention in recent years owing to the high degradation efficiency and consistent performance obtained.[22] However, the use of these light sources has serious health and environmental risks,[23] as well as power costs that limit applicability for commercialization. Because of these concerns, researchers have examined sunlight-based photocatalysis processes in the past few years, which can be both a free source of energy and sustainable.[24] The most challenging issues in the last decades in using photocatalysts for organic compound degradation have been to find an economically feasible, earth-abundant, and easy to synthesis material that has high efficiency and low toxicity.

A variety of semiconductor photocatalysts such as TiO_2 (band gap energy: 3.2 eV),[25] V_2O_5 (2.8 eV),[26] $SrTiO_3$ (3.4 eV), Fe_2O_3 (2.2 eV), ZnS (3.6 eV), SnO_2 (3.5 eV), WO_{3-x}

Received: August 13, 2020
Accepted: September 29, 2020
Published: September 29, 2020

https://dx.doi.org/10.1021/acsanm.0c02199
ACS Appl. Nano Mater. 2020, 3, 10284–10295

Table 1. Comparison of Different Wastewater Treatment Processes

items	membrane separation/membrane bioreactor[14]	activated-carbon adsorption[15]	chemical coagulation[16]	ozone oxidation[17]	Fenton method[18]	biological treatment[19]	photocatalytic methods[20]
chemical oxygen demand removal (%)	90–95	20–75	20–50	30–60	65–85	60–95	80–100
operating cost (US $/m^3)	0.4–1.0	0.3–1.1	0.1–0.4	0.7–1.0	0.3–0.7	0.5–1.5	0.2–1.2
note	treatment is necessary for concentrate	regeneration is necessary for activated carbon	treatment is necessary for sludge	treatment is necessary for wasted O_3	treatment is necessary for sludge	co-treatment is always required	treatment of catalyst is required in some cases

(2.6 to 3.0 eV), Nb_2O_5 (3.4 eV), and ZnO (3.37 eV) have been used for photocatalytic wastewater treatment systems.[27,28] Most of these materials have only been explored on the laboratory scale, although TiO_2 and ZnO have been used for commercial treatment systems as well.[29,30] Among all of these materials, ZnO shows particular promise because of its direct band gap of 3.37 eV (near-visible spectrum);[31,32] however, not all synthesized catalyst matrices perform well because of the rapid recombination of charge carriers.[33] In addition, high surface area of the catalyst is important but so too is the surface chemistry of the particle as it can increase adsorption and degradation. Among many possible structures that can be formed, it has recently been hypothesized that flake-based and flower-like ZnO materials provide high activity because of a combination of fine grain size, large surface area, and abundant mesopores.[34,35] In order to optimally employ these catalysts for the degradation of POPs in water, they must be employed on a suitable support.[46]

Recently, materials that are quite effective for separation and dye removal[36] [especially methylene blue (MB)][25,37−39] applications have been reported; however, most are not sustainable and environmentally friendly as they are based on nonbiodegradable polymers or inorganic components that are hazardous for the environment.[40] Novel and environmentally friendly material supports that enhance photocatalytic efficiency and are compatible with semiconductor catalysts are needed.[41,42] Cellulose nanofiber (CNF) biopolymers are excellent support material candidates as they are abundant, biodegradable, nontoxic, and biocompatible.[43,44] CNF by itself has a small amount of photocatalytic activity under UV or visible light irradiation; however, activity is dramatically improved and the retention of particles is enhanced by embedding semiconductor photocatalysts into the matrix.[43,45]

In this study, we report the synthesis and use of an easily prepared ZnO/CNF composite which uses sunlight, earth abundant Zn, and cellulose for the sustainable degradation of model POP MB. We measured the efficiency of MB photobleaching and compared it with existing photocatalytic composites such as ZnO, TiO_2, and Nb_2O_5.

MATERIALS AND METHODS

Materials. CNF (KY-100S grade and 25% solid content) was purchased from DAICEL Chemical Industries Limited, Japan. Zinc acetate dihydrate ($C_4H_6O_4Zn{\cdot}2H_2O$) with a purity of higher than 98% (ACS reagent) and MB dye were purchased from Sigma-Aldrich Co., Australia. Sodium hydroxide dry pellets and analytical/reagent grade absolute ethanol were procured from Merck Co., Germany, and Ajax Finechem, Australia, respectively. All materials were used without further purification.

Method. CNF (1, 1.5, and 2 wt % of dry content) was first suspended in deionized (DI) water, treated at 3000 rpm for 15,000 revolutions in a Messmer disintegrator (model MKIIIC, Netherlands), and then the suspension was homogenized using a GEA Niro Soavi homogenizer, Italy, for one pass with a pressure ranging between 600−700 psi.

The method used for the preparation of the composite was in situ precipitation, using a modification of preparation techniques described in the literature,[46−48] by varying the NaOH concentration, temperature, preparation process, and heating time. Two liter suspensions of homogenized CNF (at one of 1, 1.5, and 2 wt % CNF) were mixed at 800 rpm using a Eurostar mixer (model, IKA-Werke, Germany), followed by the addition of zinc acetate dihydrate (42, 84, 126, and 168 g to produce concentrations of 0.1, 0.2, 0.3, and 0.4 M, respectively) and mixing for 1 h. Sodium Hydroxide pellets (NaOH) were slowly added to the suspension (40, 80,120, and 160 g

https://dx.doi.org/10.1021/acsanm.0c02199
ACS Appl. Nano Mater. 2020, 3, 10284−10295

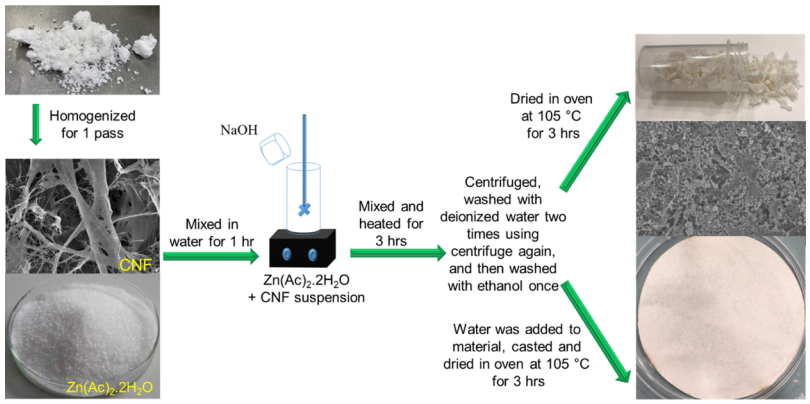

Figure 1. Summary of the in situ preparation of ZnO/CNF composite.

Table 2. ZnO/CNF Composite Loadings

sample description	abbreviation	ZnO relative wt % to total composite mass based on the balanced reaction	ZnO relative wt % to total composite mass based on experimental weight measurement	ζ potential (mV)
0.1 M $Zn(Ac)_2{\cdot}2H_2O$, 0.5 M NaCl, 1 wt % CNF of the initial suspension	IZnOCNF	45	29	−28.3
0.2 M $Zn(Ac)_2{\cdot}2H_2O$, 1 M NaCl, 1 wt % CNF of the initial suspension	IIZnOCNF	60	46	−34.9
0.3 M $Zn(Ac)_2{\cdot}2H_2O$, 1.5 M NaCl, 1 wt % CNF of the initial suspension	IIIZnOCNF	70	64	−38.0
0.4 M $Zn(Ac)_2{\cdot}2H_2O$, 2 M NaCl, 1 wt % CNF of the initial suspension	IVZnOCNF	75	72	−37.2
0.3 M $Zn(Ac)_2{\cdot}2H_2O$, 1.5 M NaCl, 1.5 wt % CNF of the initial suspension	VZnOCNF	60	58	−34.2
0.3 M $Zn(Ac)_2{\cdot}2H_2O$, 1.5 M NaCl, 2 wt % CNF of the initial suspension	VIZnOCNF	50	48	−34.2

to produce concentrations of 0.5, 1, 1.5, and 2 M), all amounts were used based on 2 L of the suspension. The amount of NaOH added was equivalent to 5 mol of NaOH/1 mol of zinc acetate dihydrate, which equates to 3 mol excess NaOH, to make sure that the reaction as indicated in eq 1 was completed. The temperature was kept constant at 80 °C throughout.

$$Zn(CH_3COO)_2{\cdot}2H_2O + 2NaOH \rightarrow ZnO + 2CH_3COONa + 3H_2O \quad (1)$$

Mixing was maintained for 3 more h at 80 °C to produce a milky suspension. The suspension containing the composite was centrifuged and the supernatant was removed. After centrifuging, 2 L of DI water was added to the remained material and centrifuged again, the supernatant was removed and this procedure was done for another time, and after that, the remained material was washed with 0.5 L of ethanol. Then, for the powder catalyst, the washed materials were dried in an oven at 105 °C. To form sheets, the washed materials with ethanol were mixed with water again, casted on stainless steel ring, and then dried in the oven at 105 °C. The overall methodology for composite production is shown in Figure 1.

The degree of completeness of the reaction was indicated by the increase in weight after washing and drying. In the case of CNF at a dry weight percentage of 1.5 wt %, the initial weight after drying was 29.5 ± 0.5 g, and the amount of the ZnO based on eq 1 for composite with 0.3 M loading of $Zn(Ac)_2{\cdot}2H_2O$ and 1.5 wt % of the total suspension of CNF should be 48.8 g of ZnO. After preparation using the in situ method described above, the change in weight of the final composite (which is = total weight − initial CNF weight) was 44.4 ± 0.5 g, which shows 91% yield of the desired ZnO nanomaterials. All experiments were carried out in triplicate. Based on eq 1, and as the complete reaction was assumed, the amount of ZnO that was added into CNF suspension for all of the samples was 16.3, 32.5, 48.8, 65.1, 48.8, and 48.8 g for IZnOCNF, IIZnOCNF, IIIZnOCNF, IVZnOCNF, VZnOCNF, and VIZnOCNF, respectively. Based upon the change in weight, the amounts of material attributed to ZnO in the composites were 10.4 ± 0.7, 24.7 ± 0.4, 44.4 ± 0.5, 62.3 ± 0.2, 46.9 ± 0.1, and 46.4 ± 0.1 g, respectively. All of the theoretical and experimental percentages of ZnO loading in all six composites are presented in Table 2 based on the ZnO weight mentioned before. Also, the abbreviations for all samples are presented in Table 2.

Characterization. The morphology of the ZnO/CNF composites was evaluated by scanning electron microscopy (SEM). The films were first sputter coated with iridium and then investigated using FEI Nova Nano-SEM 450 (FEI, USA). Energy dispersive X-ray analysis (EDX) was conducted to determine the elemental composition of the ZnO/CNF composite. For the EDX images, the FEI Nova Nano SEM 450 FEG SEM and FEI Magellan 400 FEG SEM at the Monash Centre for Electron Microscopy, Australia, were used. All of the images were captured at an acceleration voltage of 5 kV, and with increasing magnification from 250× up to 250,000×.

Small-angle X-ray scattering (SAXS) measurements were performed at the SAXS/wide-angle X-ray scattering beamline of the Australian Synchrotron using X-ray energy of 12 keV (λ = 1.033 Å). Samples were measured in the open air in transmission mode. The distance between the sample and detector was 7 m, which gives a q range of 0.001 to 0.1 A^{-1}. The X-ray photons scattered from the sample were collected by the PILATUS 1M detector (pixel size 172 μm × 172 μm). The standard silver behenate was used to calibrate the q values. Data reduction and radial averaging of the raw scattering images were made using Scatter Brain software. In SAXS, the distribution of oriented particles of different shapes shows an average anisotropic scattering depending on their sizes and arrangements in the bulk sample. The distribution of randomly oriented particles gives isotropic scattering. SAXS is a nondestructive analysis method that provides a nanostructure's shape, size, and distribution over a complete volume in the nanometer scale of 1−100 nm.[49]

The ζ-potential of all samples were measured using NanoBrook Omni (Brookhaven Instruments, USA). The samples for this test were diluted, centrifuged, and then subjected to ultrasonication (Sonics &

https://dx.doi.org/10.1021/acsanm.0c02199
ACS Appl. Nano Mater. 2020, 3, 10284−10295

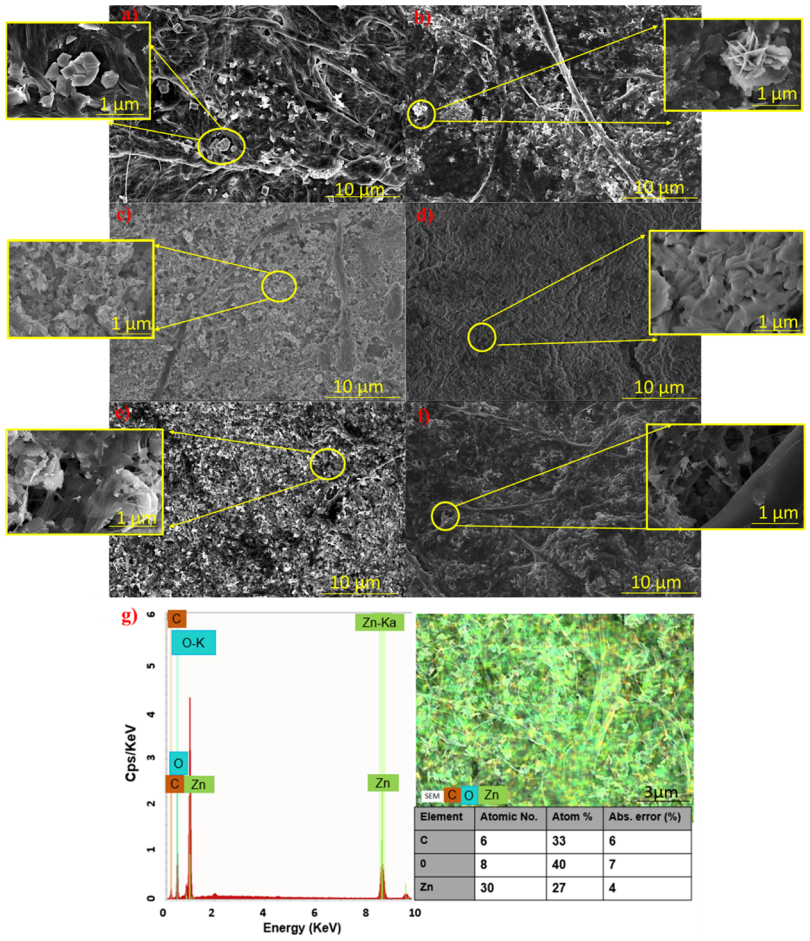

Figure 2. SEM images of in situ prepared ZnO/CNF nanocomposites used for photocatalysis with different nominal compositions (a) IZnOCNF, (b) IIZnOCNF, (c) IIIZnOCNF, (d) IVZnOCNF, (e) VZnOCNF, (f) VIZnOCNF, (g) EDX image of the in situ prepared IIIZnOCNF composite with the domain elements wt % on the surface of the composite.

Materials Inc., USA), to increase the uniformity of the fibers in the suspension. The ζ potential was measured based on the Smoluchowski equation.[50]

Fourier transform infrared (FTIR) spectra were used to investigate the chemical bonding and characterization of the composites using an Agilent Technologies Cary 630 FTIR (USA). Tests were done in the range of 600−4000 cm^{-1} with eight scans at 4 cm^{-1} resolution. A Micromeritics ASAP2420 was used for N_2 gas sorption and BET (Brunauer−Emmett−Teller) analysis. For adsorption measurements, UHP-grade (99.999% purity) N_2 was used. Samples (60−100 mg) were activated under reduced pressure for 24 h at 100 °C. To determine the sample mass within the analysis tubes, the activated and degassed samples were weighed. N_2 isotherms of samples were obtained in a liquid nitrogen bath and at 77 K in the range of 0−1 bar. To obtain the X-ray diffraction (XRD) pattern, a Bruker D8 Advance A25 X-ray Diffractometer operating under Cu Kα radiation (1.54056 λ, 40 kV, 40 mA) equipped with a Lynx Eye XE-T detector was used. All samples were scanned with a step size of 0.02° and a count time of 0.1 s per step over the 2θ range 5−100°, and were spun at 15 rpm during data collection.

The Photocatalytic Process under the UV Lamp and Sunlight. To investigate the photocatalytic properties of the composites under the UV lamp, the MB dye was used as a model pollutant. For UV lamp exposure, four 9 W lamps were employed (Nail Polish UV Light Dryer 36W Acrylic Gel Shellac Manicure Curing Lamp). These lamps provided an intensity of 1400−2000 $\mu W/cm^{-1}$ of UVA/B as measured using a ProSciTech Pty Ltd UVA/B meter model E850009, which measures the UV intensity in the range of 280−400 nm. Before starting the UV exposure, the ZnO/CNF composite (in both sheet and powder forms with loadings that will be discussed later in the Results and Discussion) was added to 100 mL of MB aqueous solution (5 mg/L, pH = 8.3) and stirred (200 rpm) for 1 h in the dark to allow adsorption−desorption to reach equilibrium. The sheet form of the composite retained its integrity, whereas the powder form composite fully dispersed in the solution. The mixture was then positioned under UV lamp irradiation and 1 mL of samples of the mixture were pipetted out every 10 min for UV/vis analysis. A similar procedure was conducted for exposure using natural sunlight between 11 AM and 12 PM (UV-index ≈ 3−5 as indicated from www.bom.gov.au website) and the UV intensity between 1500−2900 $\mu W/cm^{-1}$ of UVA/B at global positioning system location of −37.909551,145.133253. All experiments were conducted in triplicate. To investigate the effect of CNF and ZnO separately, they were used as catalyst model separately with the same procedure described for the ZnO/CNF catalyst earlier. The dye degradation rate of the pipetted solution (collected at standard intervals) was measured using an Agilent Cary 60 UV/vis Spectrophotometer and equations used for this purpose are as follows.

$$AR = ((A_0 - A_1)/A_0) \times 100 \quad (2)$$

$$DR = ((A_1 - Dt)/A_1) \times 100 \quad (3)$$

Where AR and DR are adsorption and degradation rate (%), A_0, is the absorption of dye (initial concentration of mg/L), A_1 is the absorption after 1 h adsorption under the dark box for both UV lamp and sunlight experiments, and Dt is degradation after a standard interval of irradiation (0, 10, 20, 30, 40, 50, and 60 min), respectively (all measured at the peak with the wavelength of 664 nm). To fit the data from experiments, a first-order kinetics model was used and rate

https://dx.doi.org/10.1021/acsanm.0c02199
ACS Appl. Nano Mater. 2020, 3, 10284−10295

constant values were measured by putting a very small initial guess for it (k = 0.001 min^{-1}) in each experimental data set and calculating the final rate constants in OriginLab software.

Mass spectrometry (MS) analysis was carried out at the Monash Analytical Platform, Australia (School of Chemistry, Monash University). A 10 μL injection volume of test compound was used in conjunction with a 3 min isocratic gradient of acetonitrile with 0.1% formic acid on an Agilent 1200 series LC (Santa Clara, CA, USA). Analysis was conducted on a Agilent 6450 QTOF MS system (Santa Clara, CA, USA) with a dual ESI source. The MS was operated in positive or negative mode under the following conditions: nebulizer pressure 45 psi, drying gas flow-rate 10 L/min, gas temperature 300 °C, capillary voltage 4000/−4000 V, fragmentor 180 V, and skimmer 65 V. Instrument was operated in the extended dynamic range mode with data collected in m/z range 100−1500. The detection limitation of MB in samples using MS analysis was 0.01 μg/L. All results were compared with the DI water MS results as a model and it was realized that the low intensity peaks in background are noises which appeared because of the testing conditions and are not byproducts of MB.

RESULTS AND DISCUSSION

Surface Morphology. Figure 2 shows SEM images of ZnO/CNF composites having different ZnO and CNF loading: (a) IZnOCNF, (b) IIZnOCNF, (c) IIIZnOCNF, (d) IVZnOCNF, (e) VZnOCNF, (f) VIZnOCNF. ZnO nanomaterials were distributed on the surface of the CNF matrix for all composites. We hypothesized by increasing the amount of $Zn(Ac)_2{\cdot}2H_2O$ loading, ZnO distribution on the surface of the composite will be increased and as a result, the degradation efficiency will increase, and by tacking SEM images, Figure 2a−c show the distribution of ZnO on the surface of the composite that increased with $Zn(Ac)_2{\cdot}2H_2O$ loading. The IVZnOCNF sample (Figure 2d) has been completely coated with an agglomerated ZnO layer that can be attributed to either the high ZnO content in the composite or different interactions among ZnO nanomaterials (such as polarization forces and dipole−dipole interactions).[51] Based on the results of SEM images, the size of ZnO nanomaterials are distributed between 30−500 nm and most of them are in the range of less than 200 nm.

However, by increasing the CNF content in the composite and keeping the $Zn(Ac)_2{\cdot}2H_2O$ loading constant (Figure 2e,f), more CNF were placed on the surface of the matrix. Figure 2g shows the EDX results of the in situ synthesized IIIZnOCNF composite with both elemental peaks and atomic % for zinc, carbon, and oxygen, which indicates the presence of ZnO particles on the surface of the composite. Varanasi et al.[52] investigated the in situ preparation of $CaCO_3$ nanomaterials in CNF and found that by using in situ preparation, the porosity of the matrix can be refined and managed, and as the nanomaterials are filling the pores, the adsorption rate on the surface of the composite will increase. Hence, we employed this method to enhance the adsorption of dye on the surface, which will facilitate the degradation process.

Sample Characterization. Figure S1 shows the FTIR spectra of the in situ prepared materials to evaluate the change in peaks associated with changing the composition from CNF to ZnO/CNF composites. The two main peaks at 1028 (vs) and 3317 (s) cm^{-1} are associated with the C−O and O−H ether groups stretching vibration. The peak at 1650 (w) cm^{-1} is due to the adsorbed water O−H bending. Peaks at about 2920 cm^{-1} are due to the symmetric and antisymmetric vibration of $-CH_2$ groups and the peak at 1140 (s) belongs to the stretching band of C−C ring.[53,54] The presence of two new peaks at 1395 and 1586 cm^{-1} result from symmetric and asymmetric stretching vibration of the carbon-oxygen group of acetate (C═O), which presents the anionic moieties (segments) of acetate in the ZnO/CNF matrix.[55]

To investigate the specific surface area and pore size of the prepared samples, the nitrogen adsorption (BET) analysis was done. Results are presented in Table S1. N_2 sorption isotherms showed very low surface area for CNF samples (0.1 m^2/g); however, by the addition of ZnO to the composite, the surface area increases gradually to 2.24 and 10.09 m^2/g for IZnOCNF and IIZnOCNF. Highest surface area belongs to IVZnOCNF with 12.06 m^2/g; however, because of the large amount of ZnO in the composite, CNF sites are blocked (based on the SEM images in Figure 2), which results in slower photodegradation of MB compared with the VZnOCNF samples. The photodegradation mechanism on the surface of the composite can be described as a movement of photogenerated carrier to the composite surface, which will give them enough time and space to react with water or oxygen to produce active sites. Afterward, MB dye adsorption on the catalysts surface reduces the length of the pathway the active species need to travel to have an effective reaction, and therefore enhances the photocatalytic activity. Also, pore size in the samples improves from microporous for CNF (249 nm) to mesoporous for samples with high loading of ZnO (6.9 nm for IIZnOCNF). VZnOCNF with the pore size of 3.2 nm can be called as a fine mesoporous composite.

The effect of the addition of ZnO nanomaterials on the structure and the crystallinity of CNFs was explained using XRD analysis (Figure S2). The original CNF peaks occurred at around 18 and 22°, which is consistent with the crystalline components structure.[56] The XRD pattern for the composites shows agreement with the ZnO standard pattern (JCPDS 361451), confirms the existence of ZnO nanomaterials in the structure of the composite. For all samples from IZnOCNF to VIZnOCNF except for IVZnOCNF, the peaks with the angles at around 31, 34, 35, 47, 56, 62, 67, 68, 69, and 77° corresponding to 100, 002, 101, 110, 102, 112,103, 200, and 202 ZnO planes appear from weak for IZnOCNF to strong signals for IIIZnOCNF and VZnOCNF, respectively. These strong peaks prove the presence of ZnO in the catalyst.

CNFs have almost no lignin or hemicellulose, so there is none of them in the structure of CNF to be removed. Also, as the PH was about 12, it will not have serious impact or damage on the structure and properties of CNF.

SAXS experiments were used to study the morphology and distribution of ZnO nanostructures present for in situ prepared ZnO/CNF composites. Figure S3a shows the SAXS scattering patterns for IZnOCNF, IIZnOCNF, and IIIZnOCNF. Anisotropic scattering is observed for IZnOCNF, which is consistent with the presence of mixed shapes and sizes of oriented ZnO particles as observed by SEM (Figure 2). The other two samples (IIZnOCNF and IIIZnOCNF) exhibit isotropic scattering with an increasing ZnO content.

After data reduction and radial averaging, the scattering images were converted into scattering curves, which are plotted as scattering intensity versus momentum transfer q vector. Figure S3b shows the scattering curves of pure CNF, IZnOCNF, IIZnOCNF and IIIZnOCNF. All the scattering curves including pure CNF shows the slope of $q^{-3.0}$ or $q^{-4.0}$ between q = 0.01 to 0.1 $Å^{-1}$, which is due to the surface scattering from the cellulose nanofibre bundles and the aggregated ZnO structures formed in the CNF network. At lower q < 0.01 $Å^{-1}$, all samples with ZnO show slope between

https://dx.doi.org/10.1021/acsanm.0c02199
ACS Appl. Nano Mater. 2020, 3, 10284−10295

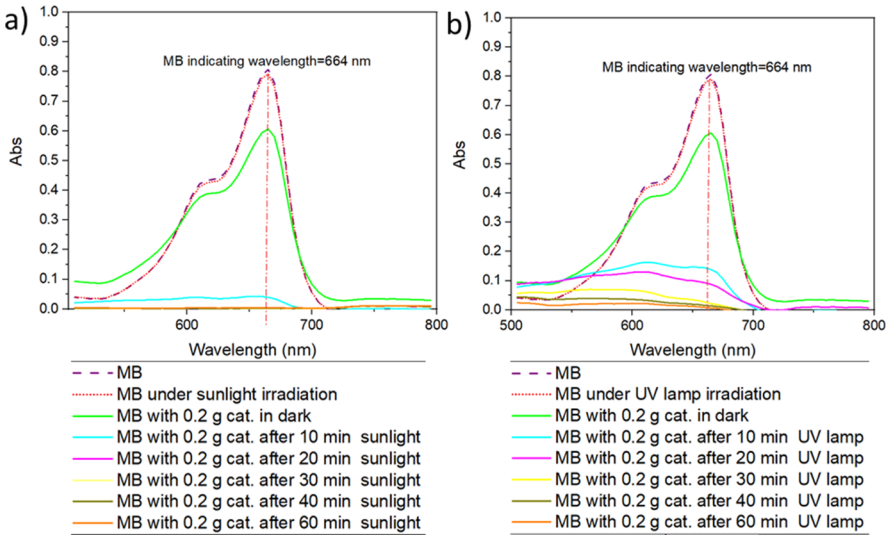

Figure 3. UV/vis spectra of MB dye solution with and without 0.2 g of the IIIZnOCNF composite per 100 mL water under (a) sunlight and (b) UV lamp as a function of irradiation time. (—— ——) represents MB solution without further treatment as a model, (····) represents MB solution without catalyst and after 60 min under sunlight irradiation, (——) represents MB solution at starting point after 60 min adsorption in the dark with catalyst, and the rest of the lines present MB solution with the catalyst under irradiation after the indicated time.

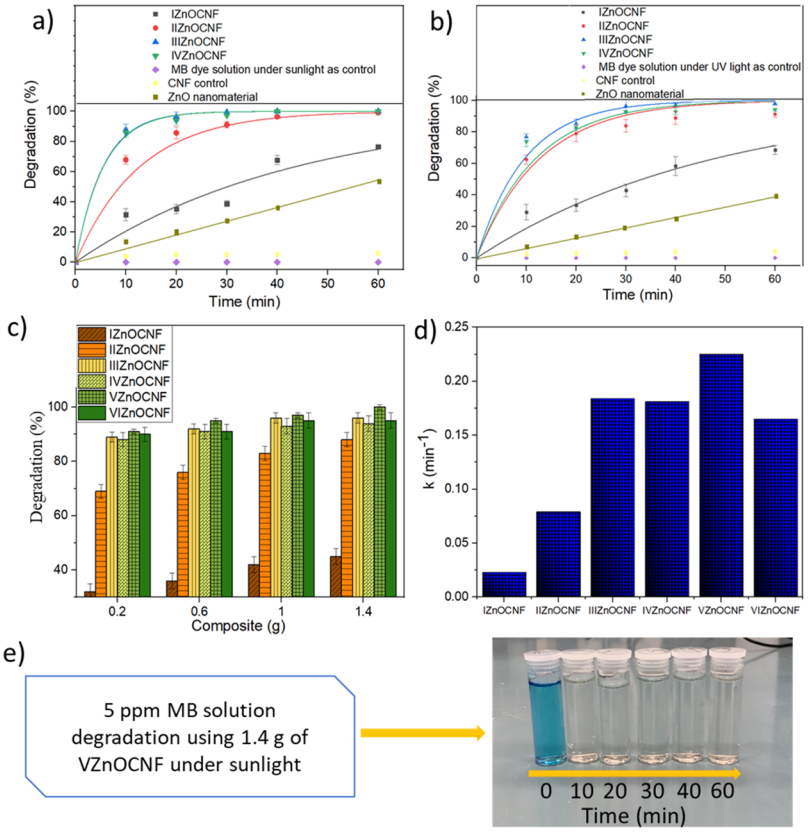

Figure 4. Degradation rate of MB dye by IZnOCNF, IIZnOCNF, IIIZnOCNF, IVZnOCNF composites (0.2 g/100 mL water): (a) sunlight (b) UV lamp; (c) varying amounts of all catalysts; after 10 min sunlight irradiation, (d) first-order rate constants for the photodegradation of MB (sunlight). (e) photograph of the sample.

$q^{-1.0}$ and $q^{-1.5}$ indicating the surface scattering from large structures of 1D and 2D shapes, which based on the SEM results are uneven shapes. The pronounced peak for the sample IIIZnOCNF at $q = 0.008$ A^{-1} in the Kratky plot (Inset) indicates the large volume fraction of similar shape and size ZnO nanostructures with the size of between 75 and 80 nm that are distributed isotropically. The IIZnOCNF sample also shows a small peak at $q = 0.0066$ $Å^{-1}$ that derives from the lower amount of ZnO nanostructures of size about 90−100 nm. No peak was observed for the IZnOCNF sample indicating the multiple shape structures are distributed anisotropically. The scattering from the pure CNF sample follows a power law consistent with surface scattering from microscale structures.

https://dx.doi.org/10.1021/acsanm.0c02199
ACS Appl. Nano Mater. 2020, 3, 10284−10295

Adsorption and Degradation of MB Dye. The adsorption and degradation of MB were examined using UV/vis analysis. Adsorption of MB onto catalyst will give time to it to catalyst to degrade the pollutants and interact with their molecules to break them which facilitate the degradation process. The positively charged MB was expected to adsorb onto the composite as a function of increasing negative charge associated with increased ZnO loading (Figure S4). Adsorption of 3×10^{-3}g MB/g CNF composite occurs in the absence of ZnO. Also, high adsorption on the ZnO surface observed which is due to the high surface area of this ZnO nanomaterial (as explained in BET results). Then, by increasing the ZnO and CNF content in the samples, the adsorption onto the composite increased up to 30×10^{-3}g MB/g composite. This may result from the ZnO particle morphology change from blocks to the flower-like and plate shape ZnO observed in the SEM images. By way of comparison to previous work of our group using TiO_2,[57] the level of adsorption increased by a factor of two (from 15×10^{-3} to 35×10^{-3}g MB/g composite), indicating a greater amount of dye on the surface of the composite, which may give more efficient photodegradation.

Additionally, the increased ZnO content imparts a more negative ζ-potential to the composite particles (−21.4 mV for CNF to −38.0 mV for IIIZnOCNF) as summarised in Table 2. However, when the ZnO content increased to beyond 64 wt % of the total mass of the composite, the adsorption of dye on the composite decreased to 34% of the total concentration of the dye solution, possibly due to the coagulation of ZnO nanomaterials at the surface of the composite (Figure 2d).

Figure 3 shows UV/vis spectra for the degradation of MB dye by an aqueous suspension of IIIZnOCNF composite under both sunlight (Figure 3a) and a UV lamp (Figure 3b). In both Figure 3a,b, the purple dashed line indicates the 5 ppm concentration MB dye solution without catalyst or light irradiation. The red dotted line is the control for 5 ppm MB solutions without a catalyst treatment but with either sunlight or UV lamp irradiation for 60 min. The green line is the control for 5 ppm MB solution mixed with the catalyst (0.2 g IIIZnOCNF/100 mL water) and kept in dark box for 60 min. These initial decrease in MB absorption arises from dye adsorption onto the catalyst particles.

Upon exposure to sunlight as a free and sustainable source of energy, the MB peak absorption in UV/vis detection decreased by >90% in 10 min and >99% photodegradation was apparent after 20 min (Figure 3a). Upon exposure to a UV lamp, the MB absorption in UV/vis detection decreased by >75% after 10 min and >96% photodegradation was observed after 30 min, and after 30 min, the rate of reduction in MB absorption changed and the absorption was slightly decreased till 60 min to >98%.

Figure 4a highlights the degradation of MB dye solutions upon treatment with sunlight for 60 min in the presence of the suspended composites. The extent of photodegradation varied as a function of composite, and using IZnOCNF, IIZnOCNF, IIIZnOCNF and IVZnOCNF, resulting in a decrease of MB absorption (in the UV/vis spectrum analysis) by 77, 98, >99 and >99%, respectively. The sample with the lowest ZnO loading (IZnOCNF) showed the least amount of photodegradation after 60 min. The fastest rate of photodegradation amongst these four composites was achieved by IIIZnOCNF and IVZnOCNF composites with 97% of MB bleached after 10 min and >99% after 20 min. Figure 4b illustrates the photodegradation of MB dye under UV lamp exposure for up to 60 min. The UV lamp resulted in about 98% photodegradation of MB and slightly less degradation for all catalysts as well as slower rates in all cases compared to the sunlight irradiation. As UV lamps had weak UV intensity compared with the sunlight, it took more time for them to help the photodegradation of the dye. Hence, the degradation lines for the system under UV lamps showed a lower rate, which finally resulted in >99% photodegradation after 60 min. ZnO and CNF were also separately investigated as models and CNF showed about 5% photodegradation after 60 min. However, ZnO showed 57 and 38% photodegradation of MB under sunlight and UV lamp, respectively.

Figure S5a shows the effect of CNF loading on the ZnO loading % and then, on the degradation of MB dye. As the CNF in the composite increased from 36 to 42, and 52, the loading of ZnO decreased from 64 (IIIZnOCNF) to 58 (VZnOCNF) and 48 (VIZnOCNF) wt % (0.3 M of $Zn(Ac)_2 \cdot 2H_2O$ and 1.5 M of NaCl were used for all three composites), and the functionality of the composites changed. With VZnOCNF, total photodegradation of the MB dye happened at around 10 min. Here, the main hypothesis was that increasing CNF until 42% could give a higher substrate to ZnO to be synthesized on the fibers and do not coagulate, which as a consequence would give more surface area to the sample to degrade the dye faster. While increasing the CNF content to 52 wt % (VIZnOCNF) did not improve the performance of the composite compared to VZnOCNF; hence, VZnOCNF was selected as the sample with the highest photodegradation functionality among all six synthesized catalysts.

The amount of degradation after 10 min of sunlight irradiation was also examined as a function of the amount of composite (Figure 4c). By increasing the amount of composite used from 0.2 to 1.4 g, the amount of photodegradation increase substantially for IZnOCNF and IIZnOCNF, but only slightly for the other samples. Hence, a full sunlight photodegradation of MB was reached in less than 10 min using 1.4 g of VZnOCNF (which is the composite with higher photodegradation rate among all prepared composites).

The rate of MB degradation was fit using a first-order kinetics model.[58]

$$kt = -\ln(C/C_0) \tag{4}$$

where k (min^{-1}) is the first-order rate constant, t (min) is the time of irradiation, C_0 is the initial concentration of MB, and C is the remaining concentration of MB in the system. To calculate the k values (Table S2), the data sets shown in Figures 4a,b and S5a,b were fitted using eq 4 (Table S2). Figure 4d shows the rate constants for MB photodegradation for all prepared catalysts under sunlight irradiation (0.2 g catalysts/100 mL water; 5 ppm MB) and based on eq 4. Although the catalyst with lowest ZnO loading and ζ potential does exhibit the lowest photodegradation rate (IZnOCNF), materials such as IIZnOCNF/VIZnOCNF with similar values exhibit a factor of two in rate difference. The differences in rate between IIIZnOCNF, IVZnOCNF, VZnOCFN, and VIZnOCFN are not simply explained by loading or zeta potential differences. For all catalysts, higher photodegradation rates (1−4%) were observed for sunlight as compared to the UV lamp with the greatest increase occurring for the most active materials (III−VI). All experiments were repeated for both powder and sheet form of catalysts and the difference between the efficiencies were less than 5% over time of usage.

https://dx.doi.org/10.1021/acsanm.0c02199
ACS Appl. Nano Mater. 2020, 3, 10284−10295

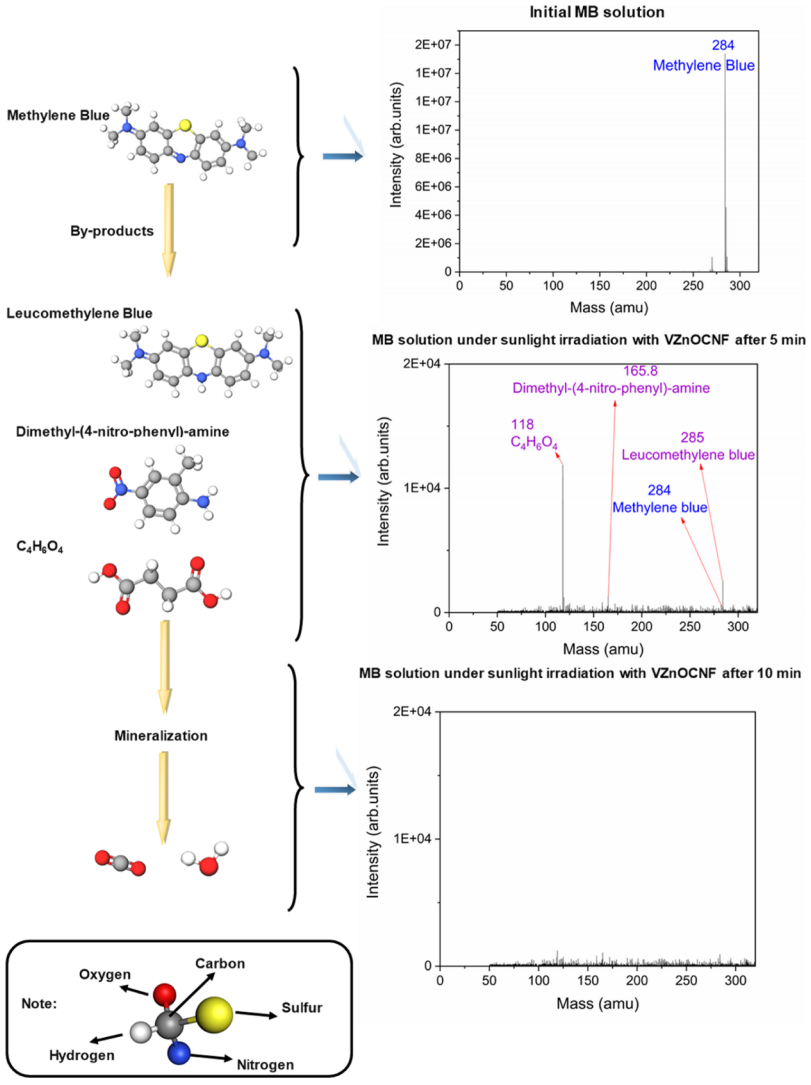

Figure 5. MS results and photocatalytic degradation pathway of the MB dye (10 ppm) using the VZnOCNF catalyst (0.2 g/100 mL water), under sunlight irradiation.

Table 3. Comparison of the Synthesized ZnO/CNF Composite with Other Metal Oxide Composite Photocatalysts in the Literature

M−O_x or composite	irradiation source	MB degradation under irradiation (%)	MB concentration (ppm)	refs
VZnOCNF	4 UV lamp-9 W-365 nm, 1400−2000 $\mu W/cm^{-1}$ of UVA, UVB	after 60 min: 94	10	this study
VZnOCNF	UV index ≈ 3−5, 1500−2900 $\mu W/cm^{-1}$ of UVA, UVB	after 10 min: >99	10	this study
ZnO@C−Ag	AM 1.5 100 mW/cm^2 simulated sunlight	after 20 min: 98	10	67
carbon-doped ZnO	500 W metal halide lamp with a 420 nm cutoff filter	after 180 min: >99	10	66
porous graphene-$SrTiO_3$	high-pressure 250 W Hg vapor lamp wavelength: 410−700 nm	after 120 min: 95	10	37
walnut-shaped hierarchical multihollow CdS microspheres/coordination polymer	8 W UV lamp wavelength: 365 nm	after 60 min: 88	1.5	38
Cu_3N nanocrystals decorated with Au nanoparticles	KRATOS, universal arc lamp supply: 250 W, 150XE	after 25 min: 95	unknown	39
wrinkled ultrathin graphitic C_3N_4 nanosheets	300 W Xe lamp wavelength: 420 nm	after 90 min: 99	100	36
TiO_2 nanofilms on polymeric substrates	9 W UVP compact UV lamp at 368 nm	after 120 min: 95	4	25
Fe_2O_3/TiO_2	visible Xe-lamp (Hamamatsu L2274, 150 W)	after 60 min: 93	10	62
amorphous niobium oxide hydrates shells	visible light: a 300 W xenon lamp	after 180 min: 72	10	63

https://dx.doi.org/10.1021/acsanm.0c02199
ACS Appl. Nano Mater. 2020, 3, 10284−10295

The photocatalytic reaction between catalyst and organic compounds usually happens on the catalyst surface, and therefore, having higher surface area will facilitate the degradation. The results of the catalyst in this study showed very high photocatalytic activity, which can be due to the high surface area of the composite.

A further investigation was performed using MS to identify products formed during the photodegradation of MB using the VZnOCNF catalyst (Figure 5). The untreated MB sample shows the molecular ion peak at m/z 284.[59,60] For the sample after 5 min of sunlight irradiation, results showed the presence of intermediate products of MB. The m/z at 285 shows the presence of Leucomethylene Blue ($C_{16}H_{19}N_3S$) with molecular structure shown in Figure 5, which is the reduced form of MB.[59,60] The peak at 165.8 m/z from dimethyl-(4-nitrophenyl)-amine ($C_6H_{10}N_2O_2$) is produced from hydroxyl radical attack at the N−S heterocyclic ring.[59,60] The peak at 118 m/z is related to $C_4H_6O_4$ molecules that are the equivalent to succinic acid produced by open-loop benzene. Finally, the MB sample irradiated for 10 min under sunlight showed no remaining intermediate product peak. Hence, the MB photodegradation pathway in this study is being shown in Figure 5. However, the sampling timeframe is important to investigate all of the byproducts during the degradation, and as the final product was the most important part of the monitoring, only one sampling was done before the complete photodegradation.

Tables 3 and S3 compare the degradation of MB under both the UV lamp and sunlight in this study to related work in the literature. Table S3 contains a broad range of literature and results, while Table 3 compares the most competitive composites with the results of this study. For the same concentration of MB in the solution (10 ppm), the catalyst of this study showed photodegradation of >99% under sunlight after only 10 min, while, Ragupathy et al.[61] used the TiO_2/cashew nutshell activated carbon as the catalyst and had 94% of photodegradation after 120 min, which is 12 times slower with lower photodegradation percentage. In other studies, Li et al.[62] and Oliveira et al.[63] used Fe_2O_3/TiO_2 and amorphous niobium oxide hydrate shell catalysts and observed the photodegradation under visible light of 93% after 60 min and 72% after 180 min, respectively. Ahmad et al.[64] and Lonkar et al.[65] used ZnO composites for the degradation of MB and reached 100% of degradation after 90 and 100 min, respectively, which is a much lower rate of degradation comparing to the results of the current study. Zhang et al.[66] studied the carbon-doped ZnO catalyst for the photodegradation of MB under UV lamps and results showed almost complete photodegradation after 180 min for their best sample, which is about 20 times slower than the catalyst in current study. Shen et al.[67] studied MB degradation under simulated sunlight using ZnO@C−Ag, which resulted in 98% degradation of the MB dye after 20 min, which shows a competitive material compared to this study; however, it still takes more time to get degraded and the preparation of the material and price is higher as well. Other studies with different types of catalysts ($SrTiO_3$,[37] CdS,[38] $ZnO/ZnFe_2O_4$,[68] Cu_3N,[39] C_3N_4[36]) for the photocatalytic degradation of MB showed no competitive or hardly competitive results by comparing them with the results of this study as all of them either spent long time or could not reach the complete degradation of the dye. Among these studies, Barman et al.[39] used Cu_3N composite as the catalyst and this catalyst is the most competitive material compared to this study, which shows about 95% degradation after 25 min; however, it is two and a half time slower than the material from this study. These results indicate that the photodegradation of MB using the catalyst in this study was more efficient and faster compared to the catalysts in the literature. In current study, we used sunlight as the source of energy for the degradation of pollutants, and prepared the mixture of flower-like/plate shape ZnO nanomaterials in the matrix. By using this method, the efficiency increased significantly. Therefore, by using a free source of energy and a fast and sustainable preparation method of catalyst, the expenses decreased and efficiency increased, which make the prepared catalyst a great and competitive candidate for the photocatalytic degradation of POPs. The reason for higher efficiency of catalysts in this study compared to state-of-the-art in the literature could be the presence of highly loaded CNF with the ZnO nanoflower/plate catalyst, which as verified by BET results, have very high surface area and therefore, provides more sites to interact with MB molecules.

The high photocatalytic activity of the synthesized samples is an advantage as compared to previously developed materials (Tables 3 and S3); however, to be sustainably applied for practical applications, the catalyst must be reusable. Degradation tests were repeated 10 times under the same set of conditions (sunlight; 60 min; 100 mL water; 10 ppm of MB) using the same VZnOCNF catalyst. After 10 runs, there was just 1% decrease in total MB photodegradation, which is well within the experimental error of the measurement.

Sustainability Aspects of the Prepared Catalyst and Process. To produce a sustainable material and process, some criteria should be considered such as the material, economy, design, market, equity, technology, and ecology, which are bottom lines of three main concepts of sustainability: environmental issues, social concern, and economic viability.[10−13] The materials and method developed here meet almost all of the criteria of a sustainable process and material.

(1) Material: both raw materials are earth-abundant and usage of them will not harm the environment. ZnO as a metal oxide with low toxicity is a great candidate for an environmentally friendly process. Cellulose is a renewable material, which is the most abundant biopolymer on earth. Usage of catalyst that is a long-lasting material and has long-term performance in another positive point of the materials prepared in this study. (2) Economy: both the raw materials are frequently accessible and cheap, which make them a strong candidate for usage. In addition, sunlight is a free source of energy, which will reduce the purchase and running costs during the process. (3) Design: CNF is a recyclable material and have low environmental impact as the catalyst is being made on a cellulose-based material. (4) Market: usage of two materials (CNF and ZnO) which are earth-abundant, also sunlight as the source of energy will make this study a process that can be locally deployed everywhere with minimal equipment. (5) Equity: low impact technology designed for local use to mitigate local problems. (6) Technology: production of catalyst is a new method, which introduces a new technology. Also, the technology was evaluated by conducting photodegradation tests under sunlight and developed by improving the efficiency using optimized catalysts. (7) Ecology: the manufacturing process was a low toxicity process which used almost no harmful materials to eliminate harmful pollutants in the water. Hence, these factors indicate that this study is toward sustainability.

https://dx.doi.org/10.1021/acsanm.0c02199
ACS Appl. Nano Mater. 2020, 3, 10284−10295

CONCLUSIONS

In summary, a novel series of ZnO/CNF composites with in situ precipitation of ZnO nanomaterials into the CNF matrix were prepared, examined, and studied under both sunlight and UV lamp irradiation. By combining the properties of ZnO and CNF, the resultant composite remarkably increased its efficiency in MB photodegradation under sunlight irradiation. Also, it was concluded that three main concepts of sustainability which are environment, social concern and equity, and economic viability was met in this study. Although this study showed the preparation of catalysts with high photodegradation efficiency of MB dye, more researches should be done in the future on other types of POP and using different approaches such as using a continuous photodegradation system.

ASSOCIATED CONTENT

Supporting Information

The Supporting Information is available free of charge at https://pubs.acs.org/doi/10.1021/acsanm.0c02199.

FTIR analysis of all prepared ZnO/CNF catalyst; SAXS analysis of IZnOCNF, IIZnOCNF, IZnOCNFIII, and CNF; adsorption experiment results; photodegradation results of MB dye by 0.2 g of catalyst/100 mL of water for IVZnOCNF, VZnOCNF, VIZnOCNF composites under sunlight and a UV lamp and different MB concentrations with the VZnOCNF catalyst; detailed pseudo first-order kinetic rate constants (k) table; and comparison table of MB photodegradation results with the state of the art in the literature (PDF)

AUTHOR INFORMATION

Corresponding Author

Warren Batchelor − *Bioresource Processing Research Institute of Australia, Department of Chemical Engineering, Monash University, Melbourne, Victoria 3800, Australia;* orcid.org/0000-0001-6880-7765; Email: Warren.Batchelor@monash.edu

Authors

Mostafa Dehghani − *Bioresource Processing Research Institute of Australia, Department of Chemical Engineering, Monash University, Melbourne, Victoria 3800, Australia;* orcid.org/0000-0001-5019-725X

Humayun Nadeem − *Bioresource Processing Research Institute of Australia, Department of Chemical Engineering, Monash University, Melbourne, Victoria 3800, Australia*

Vikram Singh Raghuwanshi − *Bioresource Processing Research Institute of Australia, Department of Chemical Engineering, Monash University, Melbourne, Victoria 3800, Australia*

Hamidreza Mahdavi − *Department of Chemical Engineering, Monash University, Melbourne, Victoria 3800, Australia*

Mark M. Banaszak Holl − *Bioresource Processing Research Institute of Australia, Department of Chemical Engineering, Monash University, Melbourne, Victoria 3800, Australia;* orcid.org/0000-0001-7759-7456

Complete contact information is available at: https://pubs.acs.org/10.1021/acsanm.0c02199

Notes

The authors declare no competing financial interest.

ACKNOWLEDGMENTS

The authors would like to extend their gratitude to the Australian Research Council and The ARC Research Hub for Processing Lignocellulosics into High Value Products (PALS) for financial support through the Industry Transformation Research Hub grant for this research work (grant: IH170100020). The authors are thankful to the facilities used within the Monash Centre for Electron Microscopy, Monash Analytical Platform, and Monash X-Ray Platform. Also, the authors are grateful for the help of emeritus Prof. Robert Johnson in reviewing and revising the paper, and to Monash University and the Bioprocessing Research Institute of Australia (BioPRIA) for their financial and facility support.

REFERENCES

(1) Gehr, R. L. *Theory and Practice of Water and Wastewater Treatment*: Wiley-Blackwell, 2018.

(2) Chen, G. Electrochemical technologies in wastewater treatment. *Sep. Purif. Technol.* **2004**, *38*, 11−41.

(3) Mozia, S. Photocatalytic membrane reactors (PMRs) in water and wastewater treatment. A review. *Sep. Purif. Technol.* **2010**, *73*, 71−91.

(4) Lv, Y.; Zhang, C.; He, A.; Yang, S.-J.; Wu, G.-P.; Darling, S. B.; Xu, Z.-K. Photocatalytic Nanofiltration Membranes with Self-Cleaning Property for Wastewater Treatment. *Adv. Funct. Mater.* **2017**, *27*, 1700251.

(5) Dey, T. Magnetic nanoparticles and cellulosic nanofibers to remove arsenic and other heavy metals from water. *Nanotechnology for Water Purification*; Universal-Publishers: Florida, 2012; pp 1−28.

(6) Heimer, B. W.; Paap, S. M.; Sasan, K.; Brady, P. V.; Nenoff, T. M. 110th Anniversary: Industrial process water treatment and reuse enabled by selective ion exchange materials. *Ind. Eng. Chem. Res.* **2019**, *58*, 14873−14879.

(7) Wang, Z.; Xue, M.; Huang, K.; Liu, Z. Textile dyeing wastewater treatment. *Advances in Treating Textile Effluent*; InTech, 2011.

(8) Lee, K. M.; Lai, C. W.; Ngai, K. S.; Juan, J. C. Recent developments of zinc oxide based photocatalyst in water treatment technology: a review. *Water Res.* **2016**, *88*, 428−448.

(9) Ran, J.; Ma, T. Y.; Gao, G.; Du, X.-W.; Qiao, S. Z. Porous P-doped graphitic carbon nitride nanosheets for synergistically enhanced visible-light photocatalytic H_2 production. *Energy Environ. Sci.* **2015**, *8*, 3708−3717.

(10) Bakshi, B. R.; Gutowski, T. G.; Sekulic, D. P. Claiming sustainability: requirements and challenges. *ACS Sustainable Chem. Eng.* **2018**, *6*, 3632−3639.

(11) Mousavi-Nasab, S. H.; Sotoudeh-Anvari, A. A new multi-criteria decision making approach for sustainable material selection problem: A critical study on rank reversal problem. *J. Cleaner Prod.* **2018**, *182*, 466−484.

(12) Ljungberg, L. Y. Materials selection and design for development of sustainable products. *Mater. Des.* **2007**, *28*, 466−479.

(13) Zarandi, M. H. F.; Mansour, S.; Hosseinijou, S. A.; Avazbeigi, M. A material selection methodology and expert system for sustainable product design. *Int. J. Adv. Des. Manuf. Technol.* **2011**, *57*, 885−903.

(14) Neoh, C. H.; Noor, Z. Z.; Mutamim, N. S. A.; Lim, C. K. Green technology in wastewater treatment technologies: integration of membrane bioreactor with various wastewater treatment systems. *Chem. Eng. J.* **2016**, *283*, 582−594.

(15) Rafatullah, M.; Ahmad, T.; Ghazali, A.; Sulaiman, O.; Danish, M.; Hashim, R. Oil palm biomass as a precursor of activated carbons: a review. *Crit. Rev. Environ. Sci. Technol.* **2013**, *43*, 1117−1161.

(16) Verma, A. K.; Dash, R. R.; Bhunia, P. A review on chemical coagulation/flocculation technologies for removal of colour from textile wastewaters. *J. Environ. Manage.* **2012**, *93*, 154−168.

(17) Lee, C. O.; Howe, K. J.; Thomson, B. M. Ozone and biofiltration as an alternative to reverse osmosis for removing PPCPs

and micropollutants from treated wastewater. *Water Res.* **2012**, *46*, 1005−1014.
(18) Bagal, M. V.; Gogate, P. R. Wastewater treatment using hybrid treatment schemes based on cavitation and Fenton chemistry: a review. *Ultrason. Sonochem.* **2014**, *21*, 1−14.
(19) Durai, G.; Rajasimman, M. Biological Treatment of Tannery Wastewater- A Review. *J. Environ. Sci. Technol.* **2011**, *4*, 1−17.
(20) Han, F.; Kambala, V. S. R.; Srinivasan, M.; Rajarathnam, D.; Naidu, R. Tailored titanium dioxide photocatalysts for the degradation of organic dyes in wastewater treatment: a review. *Appl. Catal., A* **2009**, *359*, 25−40.
(21) Natarajan, S.; Bajaj, H. C.; Tayade, R. J. Recent advances based on the synergetic effect of adsorption for removal of dyes from waste water using photocatalytic process. *J. Environ. Sci.* **2018**, *65*, 201−222.
(22) Al-Mamun, M. R.; Kader, S.; Islam, M. S.; Khan, M. Z. H. Photocatalytic activity improvement and application of UV-TiO2 photocatalysis in textile wastewater treatment: a review. *J. Environ. Chem. Eng.* **2019**, *7*, 103248.
(23) Ivanov, I. V.; Mappes, T.; Schaupp, P.; Lappe, C.; Wahl, S. Ultraviolet radiation oxidative stress affects eye health. *J. Biophotonics* **2018**, *11*, No. e201700377.
(24) Dinkova-Kostova, A. T.; Jenkins, S. N.; Fahey, J. W.; Ye, L.; Wehage, S. L.; Liby, K. T.; Stephenson, K. K.; Wade, K. L.; Talalay, P. Protection against UV-light-induced skin carcinogenesis in SKH-1 high-risk mice by sulforaphane-containing broccoli sprout extracts. *Cancer Lett.* **2006**, *240*, 243−252.
(25) Maleki, H.; Bertola, V. TiO_2 Nanofilms on Polymeric Substrates for the Photocatalytic Degradation of Methylene Blue. *ACS Appl. Nano Mater.* **2019**, *2*, 7237−7244.
(26) Saravanan, R.; Gupta, V. K.; Mosquera, E.; Gracia, F. Preparation and characterization of V_2O_5/ZnO nanocomposite system for photocatalytic application. *J. Mol. Liq.* **2014**, *198*, 409−412.
(27) Sheikh, M.; Pazirofteh, M.; Dehghani, M.; Asghari, M.; Rezakazemi, M.; Valderrama, C.; Cortina, J.-L. Application of ZnO nanostructures in ceramic and polymeric membranes for water and wastewater technologies: A review. *Chem. Eng. J.* **2019**, *391*, 123475.
(28) Ji, B.; Zhang, J.; Zhang, C.; Li, N.; Zhao, T.; Chen, F.; Hu, L.; Zhang, S.; Wang, Z. Vertically aligned ZnO@ ZnS nanorod chip with improved photocatalytic activity for antibiotics degradation. *ACS Appl. Nano Mater.* **2018**, *1*, 793−799.
(29) Hussein, F. H.; Abass, T. A. Photocatalytic treatment of textile industrial wastewater. *Int. J. Chem.* **2010**, *8*, 1353−1364.
(30) Miranda-García, N.; Suárez, S.; Sánchez, B.; Coronado, J. M.; Malato, S.; Maldonado, M. I. Photocatalytic degradation of emerging contaminants in municipal wastewater treatment plant effluents using immobilized TiO_2 in a solar pilot plant. *Appl. Catal., B* **2011**, *103*, 294−301.
(31) Behnajady, M.; Modirshahla, N.; Hamzavi, R. Kinetic study on photocatalytic degradation of C.I. Acid Yellow 23 by ZnO photocatalyst. *J. Hazard. Mater.* **2006**, *133*, 226−232.
(32) Choudhary, M. K.; Kataria, J.; Sharma, S. Novel green biomimetic approach for preparation of highly stable Au-ZnO heterojunctions with enhanced photocatalytic activity. *ACS Appl. Nano Mater.* **2018**, *1*, 1870−1878.
(33) Abid, M.; Bouattour, S.; Ferraria, A. M.; Conceição, D. S.; Carapeto, A. P.; Vieira Ferreira, L. F.; Botelho do Rego, A. M.; Chehimi, M. M.; Rei Vilar, M.; Boufi, S. Facile functionalization of cotton with nanostructured silver/titania for visible-light plasmonic photocatalysis. *J. Colloid Interface Sci.* **2017**, *507*, 83−94.
(34) Cao, M.; Wang, F.; Zhu, J.; Zhang, X.; Qin, Y.; Wang, L. Shape-controlled synthesis of flower-like ZnO microstructures and their enhanced photocatalytic properties. *Mater. Lett.* **2017**, *192*, 1−4.
(35) Promdet, P.; Quesada-Cabrera, R.; Sathasivam, S.; Li, J.; Jiamprasertboon, A.; Guo, J.; Taylor, A.; Carmalt, C. J.; Parkin, I. P. High defect nanoscale ZnO films with polar facets for enhanced photocatalytic performance. *ACS Appl. Nano Mater.* **2019**, *2*, 2881−2889.
(36) Gao, M.; Feng, J.; Zhang, Z.; Gu, M.; Wang, J.; Zeng, W.; Lv, Y.; Ren, Y.; Wei, T.; Fan, Z. Wrinkled Ultrathin Graphitic C_3N_4 Nanosheets for Photocatalytic Degradation of Organic Wastewater. *ACS Appl. Nano Mater.* **2018**, *1*, 6733−6741.
(37) Bantawal, H.; Sethi, M.; Shenoy, U. S.; Bhat, D. K. Porous Graphene Wrapped $SrTiO_3$ Nanocomposite: Sr−C Bond as an Effective Coadjutant for High Performance Photocatalytic Degradation of Methylene Blue. *ACS Appl. Nano Mater.* **2019**, *2*, 6629−6636.
(38) Thakur, S.; Das, P.; Mandal, S. K. Solvent-Induced Diversification of CdS Nanostructures for Photocatalytic Degradation of Methylene Blue. *ACS Appl. Nano Mater.* **2020**, *3*, 5645−5655.
(39) Barman, D.; Paul, S.; Ghosh, S.; De, S. K. Cu_3N Nanocrystals Decorated with Au Nanoparticles for Photocatalytic Degradation of Organic Dyes. *ACS Appl. Nano Mater.* **2019**, *2*, 5009−5019.
(40) Singh, S.; Singh, P.; Mahalingam, H. A novel and effective strewn polymer-supported titanium dioxide photocatalyst for environmental remediation. *J. Mater. Environ. Sci.* **2015**, *6*, 349−358.
(41) Tan, X.-f.; Liu, Y.-g.; Gu, Y.-l.; Xu, Y.; Zeng, G.-m.; Hu, X.-j.; Liu, S.-b.; Wang, X.; Liu, S.-m.; Li, J. Biochar-based nano-composites for the decontamination of wastewater: a review. *Bioresour. Technol.* **2016**, *212*, 318−333.
(42) Väisänen, T.; Haapala, A.; Lappalainen, R.; Tomppo, L. Utilization of agricultural and forest industry waste and residues in natural fiber-polymer composites: A review. *Waste Manage.* **2016**, *54*, 62−73.
(43) Liu, R.; Dai, L.; Si, C.-L. Mussel-inspired cellulose-based nanocomposite fibers for adsorption and photocatalytic degradation. *ACS Sustainable Chem. Eng.* **2018**, *6*, 15756−15763.
(44) Valencia, L.; Kumar, S.; Nomena, E. M.; Salazar-Alvarez, G.; Mathew, A. P. In-situ Growth of Metal Oxide Nanoparticles on Cellulose Nanofibrils for Dye Removal and Antimicrobial Applications. *ACS Appl. Nano Mater.* **2020**, *3*, 7172−7181.
(45) Varanasi, S.; Garusinghe, U.; Simon, G. P.; Garnier, G.; Batchelor, W. Novel In-situ Precipitation Process to Engineer Low Permeability Porous Composite. *Sci. Rep.* **2018**, *8*, 10747.
(46) Zhou, X.; Li, X.; Gao, Y.; Li, L.; Huang, L.; Ye, J. Preparation and characterization of 2D ZnO nanosheets/regenerated cellulose photocatalytic composite thin films by a two-step synthesis method. *Mater. Lett.* **2019**, *234*, 26−29.
(47) Ali, A.; Mannan, A.; Hussain, I.; Hussain, I.; Zia, M. Effective removal of metal ions from aquous solution by silver and zinc nanoparticles functionalized cellulose: Isotherm, kinetics and statistical supposition of process. *Environ. Nanotechnol. Monit. Manag.* **2018**, *9*, 1−11.
(48) Lefatshe, K.; Muiva, C. M.; Kebaabetswe, L. P. Extraction of nanocellulose and in-situ casting of ZnO/cellulose nanocomposite with enhanced photocatalytic and antibacterial activity. *Carbohydr. Polym.* **2017**, *164*, 301−308.
(49) Raghuwanshi, V. S.; Garusinghe, U. M.; Ilavsky, J.; Batchelor, W. J.; Garnier, G. Effect of nanoparticles size and polyelectrolyte on nanoparticles aggregation in a cellulose fibrous matrix. *J. Colloid Interface Sci.* **2018**, *510*, 190−198.
(50) Sze, A.; Erickson, D.; Ren, L.; Li, D. Zeta-potential measurement using the Smoluchowski equation and the slope of the current−time relationship in electroosmotic flow. *J. Colloid Interface Sci.* **2003**, *261*, 402−410.
(51) Wang, S.-S.; Xu, A.-W. Template-free facile solution synthesis and optical properties of ZnO mesocrystals. *CrystEngComm* **2013**, *15*, 376−381.
(52) Varanasi, S.; Garusinghe, U.; Simon, G. P.; Garnier, G.; Batchelor, W. Novel In-situ Precipitation Process to Engineer Low Permeability Porous Composite. *Sci. Rep.* **2018**, *8*, 10747.
(53) Ma, L.; Zhang, Y.; Wang, S. Modified treatment for carbonized cellulose nanofiber application in composites. *Composites, Part A* **2016**, *90*, 786−793.
(54) Soni, B.; Hassan, E. B.; Mahmoud, B. Chemical isolation and characterization of different cellulose nanofibers from cotton stalks. *Carbohydr. Polym.* **2015**, *134*, 581−589.

https://dx.doi.org/10.1021/acsanm.0c02199
ACS Appl. Nano Mater. 2020, 3, 10284−10295

(55) Ullah, R.; Dutta, J. Photocatalytic degradation of organic dyes with manganese-doped ZnO nanoparticles. *J. Hazard. Mater.* **2008**, *156*, 194−200.
(56) Ye, S.; Zhang, D.; Liu, H.; Zhou, J. ZnO nanocrystallites/cellulose hybrid nanofibers fabricated by electrospinning and solvothermal techniques and their photocatalytic activity. *J. Appl. Polym. Sci.* **2011**, *121*, 1757−1764.
(57) Garusinghe, U. M.; Raghuwanshi, V. S.; Batchelor, W.; Garnier, G. Water resistant cellulose−titanium dioxide composites for photocatalysis. *Sci. Rep.* **2018**, *8*, 2306.
(58) Jiang, L.; Yuan, X.; Zeng, G.; Wu, Z.; Liang, J.; Chen, X.; Leng, L.; Wang, H.; Wang, H. Metal-free efficient photocatalyst for stable visible-light photocatalytic degradation of refractory pollutant. *Appl. Catal., B* **2018**, *221*, 715−725.
(59) Gnaser, H.; Savina, M. R.; Calaway, W. F.; Tripa, C. E.; Veryovkin, I. V.; Pellin, M. J. Photocatalytic degradation of methylene blue on nanocrystalline TiO_2: surface mass spectrometry of reaction intermediates. *Int. J. Mass Spectrom.* **2005**, *245*, 61−67.
(60) Wang, X.-q.; Han, S.-f.; Zhang, Q.-w.; Zhang, N.; Zhao, D.-d. Photocatalytic oxidation degradation mechanism study of methylene blue dye waste water with GR/iTiO_2. *MATEC Web of Conferences*; EDP Sciences, 2018; p 03006.
(61) Ragupathy, S.; Raghu, K.; Prabu, P. Synthesis and characterization of TiO_2 loaded cashew nut shell activated carbon and photocatalytic activity on BG and MB dyes under sunlight radiation. *Spectrochim. Acta, Part A* **2015**, *138*, 314−320.
(62) Li, R.; Jia, Y.; Bu, N.; Wu, J.; Zhen, Q. Photocatalytic degradation of methyl blue using Fe_2O_3/TiO_2 composite ceramics. *J. Alloys Compd.* **2015**, *643*, 88−93.
(63) Oliveira, L. C. A.; Oliveira, H. S.; Mayrink, G.; Mansur, H. S.; Mansur, A. A. P.; Moreira, R. L. One-pot synthesis of CdS@ Nb_2O_5 core−shell nanostructures with enhanced photocatalytic activity. *Appl. Catal., B* **2014**, *152*−*153*, 403−412.
(64) Ahmad, M.; Ahmed, E.; Hong, Z. L.; Xu, J. F.; Khalid, N. R.; Elhissi, A.; Ahmed, W. A facile one-step approach to synthesizing ZnO/graphene composites for enhanced degradation of methylene blue under visible light. *Appl. Surf. Sci.* **2013**, *274*, 273−281.
(65) Lonkar, S. P.; Pillai, V. V.; Alhassan, S. M. Facile and scalable production of heterostructured ZnS-ZnO/Graphene nano-photocatalysts for environmental remediation. *Sci. Rep.* **2018**, *8*, 13401.
(66) Zhang, X.; Qin, J.; Hao, R.; Wang, L.; Shen, X.; Yu, R.; Limpanart, S.; Ma, M.; Liu, R. Carbon-doped ZnO nanostructures: facile synthesis and visible light photocatalytic applications. *J. Phys. Chem. C* **2015**, *119*, 20544−20554.
(67) Shen, Z.; Liang, P.; Wang, S.; Liu, L.; Liu, S. Green synthesis of carbon-and silver-modified hierarchical ZnO with excellent solar light driven photocatalytic performance. *ACS Sustainable Chem. Eng.* **2015**, *3*, 1010−1016.
(68) Liu, H.; Han, C.; Shao, C.; Yang, S.; Li, X.; Li, B.; Li, X.; Ma, J.; Liu, Y. ZnO/$ZnFe_2O_4$ Janus Hollow Nanofibers with Magnetic Separability for Photocatalytic Degradation of Water-Soluble Organic Dyes. *ACS Appl. Nano Mater.* **2019**, *2*, 4879−4890.

https://dx.doi.org/10.1021/acsanm.0c02199
ACS Appl. Nano Mater. 2020, 3, 10284−10295